Journal of the European Ceramic Society 37 (2017) 3131–3136

Contents lists available at www.sciencedirect.com

Journal of the European Ceramic Society

journal homepage: www.elsevier.com/locate/jeurceramsoc

Feature article

Low thermal conductivity of atomic layer deposition yttria-stabilized zirconia (YSZ) thin films for thermal insulation applications

Jungwan Cho[a,*], Joonsuk Park[b], Jihwan An[c,*]

[a] Department of Mechanical Engineering, Kyung Hee University, 1732 Deogyeong-daero, Giheung-gu, Yongin-si, Gyeonggi-do, 17104, Republic of Korea
[b] Department of Materials Science and Engineering, Stanford University, Stanford, CA 94305, United States
[c] Manufacturing Systems and Design Engineering Programme, Seoul National University of Science and Technology, Seoul 139-743, Republic of Korea

ARTICLE INFO

Article history:
Received 16 October 2016
Received in revised form 6 March 2017
Accepted 21 March 2017
Available online 3 April 2017

Keywords:
Yttria-stabilized zirconia (YSZ)
Atomic layer deposition
Thermal insulation applications
Thermal conductivity
Time-domain thermoreflectance

ABSTRACT

Thermal insulation applications have long required materials with low thermal conductivity, and one example is yttria (Y_2O_3)-stabilized zirconia (ZrO_2) (YSZ) as thermal barrier coatings used in gas turbine engines. Although porosity has been a route to the low thermal conductivity of YSZ coatings, nonporous and conformal coating of YSZ thin films with low thermal conductivity may find a great impact on various thermal insulation applications in nanostructured materials and nanoscale devices. Here, we report on measurements of the thermal conductivity of atomic layer deposition-grown, nonporous YSZ thin films of thickness down to 35 nm using time-domain thermoreflectance. We find that the measured thermal conductivities are 1.35–1.5 $W m^{-1} K^{-1}$ and do not strongly vary with film thickness. Without any reduction in thermal conductivity associated with porosity, the conductivities we report approach the minimum, amorphous limit, 1.25 $W m^{-1} K^{-1}$, predicted by the minimum thermal conductivity model.

1. Introduction

Yttria (Y_2O_3)-stabilized zirconia (ZrO_2) (YSZ) is a widely used material in a variety of applications due to their range of properties, such as low thermal conductivity (similar to that of a glass), high chemical stability, and high ionic conductivity [1–4]. One popular example is the use of YSZ ceramics as thermal barrier coatings, which are primarily targeted to insulate and protect turbine and combustor engine components from combusting flows and thereby enhance the performance and durability of these engines [1,2]. Because low thermal conductivity is critical in thermal insulation applications, numerous efforts have focused on reducing the thermal conductivity of YSZ coatings [1,2,5–8]. These coatings are typically 100 μm to 2 mm thick and contain a large volume fraction of porosity [1,2,8].

Of recent interest are nonporous YSZ thin films with thicknesses on the order of 100 nm, grown by radio-frequency (RF) sputtering, atomic layer deposition (ALD) and other fabrication techniques, as solid-state electrolytes for solid oxide fuel cells operating at low temperatures (~300 °C) [3,4]. Compared to other fabrication techniques, ALD can offer uniform and conformal coating of the surface of three-dimensional structured micro- and nanoscale devices [3]. Many attempts have been made to grow YSZ electrolyte films by ALD and characterize their microstructural features and electrochemical performance [3,4]. But less is known about the thermal properties of these films.

In this work, we measure the thermal conductivity of ALD-grown, nonporous YSZ thin films with three different thicknesses (35, 61, and 138 nm) using time-domain thermoreflectance (TDTR) at room temperature. We find that the measured thermal conductivities are 1.35–1.5 $W m^{-1} K^{-1}$ and do not significantly depend on film thickness. The thermal conductivities we observe here are higher than the lowest reported for highly porous YSZ ceramics—0.06 $W m^{-1} K^{-1}$ with 77% porosity [8]—but are still low in the sense that they approach the minimum, amorphous limit, 1.25 $W m^{-1} K^{-1}$, predicted by the minimum thermal conductivity model [9] without any effects associated with porosity. To the best of our knowledge, the thermal conductivities measured here are the lowest ever reported for nonporous YSZ. Considering that ALD is particularly useful for uniform and conformal coating of the surface of three-dimensional nanostructures, the findings presented here may point to the possibility of using ALD YSZ for various thermal insulation applications in nanostructured materials and nanoscale electronic and energy conversion devices.

* Corresponding authors.
E-mail addresses: jungwan.cho@khu.ac.kr, jungwan.cho@gmail.com (J. Cho), jihwanan@seoultech.ac.kr (J. An).

http://dx.doi.org/10.1016/j.jeurceramsoc.2017.03.045
0955-2219/

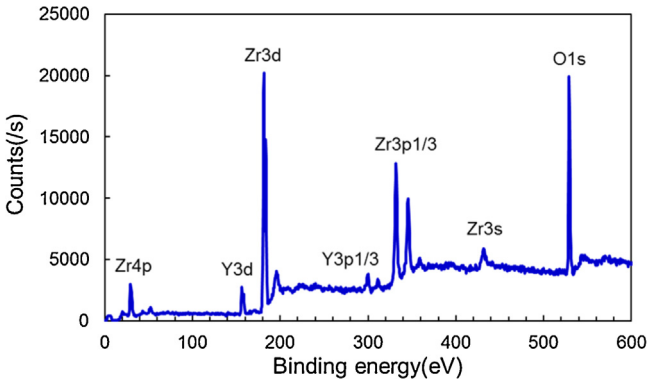

Fig. 1. XPS spectra of ALD YSZ films used in this study.

2. Material and methods

Three YSZ films of thickness 35, 61, and 138 nm are grown on p-doped Si substrates using ALD at a deposition temperature of 250 °C. The precursors used for ALD fabrication of YSZ are tetrakis-(dimethylamido) zirconium ($Zr(NMe_2)_4$) (Sigma Aldrich) for depositing zirconia and tris-(methylcyclopentadienyl) yttrium ($Y(MeCp)_3$) (Strem Chemical) for yttria. Water is used as the oxidant for both precursors. Seven zirconia deposition cycles and one yttria cycle constitute one super cycle, whose growth rate is ~9–10 Å/supercycle. The number of supercycles for 35, 61, and 138 nm films are 35, 70, and 140, respectively. A 53–56 nm Al film that is typically referred to as a transducer layer for thermoreflectance measurements is electron-beam evaporated on the surface of the three YSZ films after an extended air break.

Prior to the deposition of the Al transducer layer, the stoichiometry of the ALD YSZ films is analyzed by X-ray photoelectron spectroscopy (XPS) in a SSI S-probe monochromatized XPS spectrometer with Al KR radiation (1486 eV) (Fig. 1). The composition of the ALD YSZ films is Zr 30.0%, Y 5.5%, and O 64.5%; the doping level, i.e., x in $(Y_2O_3)_x(ZrO_2)_{1-x}$, is therefore 8.4 mol%. The possible impurities, *i.e.*, C and N, in the films were not detectible, which means their concentrations are less than 0.1 at.% (detection limit of XPS).

The crystalline phase and quality as well as the thicknesses of the ALD YSZ films are analyzed by transmission electron microscopy (TEM). The film thicknesses are measured to be 35, 61, and 138 nm. TEM images show that our films are mostly polycrystalline with nanoscale grains, i.e., nanocrystalline, with some portion of an amorphous matrix. The average grain size is ~10 nm in width (Fig. 2(a)–(f)). Lattice fringe measurement, as well as the selective area diffraction (SAD) pattern (Fig. 2(g)), confirms that our films are polycrystalline. The crystal structure of our films is dominantly tetragonal. A previous study reported that a mixture of tetragonal and cubic phases exists in 8 mol% ALD YSZ films deposited at 400 °C [10]. The relatively low deposition temperature of our films (250 °C) could be the reason why the metastable tetragonal phase is dominant in our films, although the cubic phase is the most stable phase in heavily-doped YSZ (7–10 mol%) [11]. We observe no significant change in crystallinity of films with increasing film thickness.

The thermal conductivities of the three ALD YSZ films are measured at room temperature using TDTR, an ultrafast, optical pump-probe technique based on thermoreflectance [12–14]. The output of a mode-locked Nd:YVO_4 laser (λ = 1064 nm and t = 9.2 ps optical pulses at a repetition rate of 82 MHz) is split into the pump (heater) and probe (thermometer) beams, which are concentrically focused on the sample surface using a 20× microscope objective lens. The frequency-doubled 532 nm pump beam, modulated at 6 MHz using an electro-optic modulator for lock-in detection, locally heats the sample. The time-delayed, unmodulated 1064 nm probe beam measures the time-evolution of the surface temperature through the temperature-induced changes in the reflectivity of Al. The topmost Al transducer layer acts as the pump absorber and probe reflector; i.e., it absorbs and converts the electromagnetic energy of the pump pulses into heat, and it reflects the probe pulses and generates the measurable transient surface temperature decay signal via its large coefficient of thermoreflectance at the probe wavelength. The temperature-induced changes in the reflected probe intensity are recorded by a radio-frequency lock-in amplifier at the pump modulation frequency as a function of delay time between the pump and probe beams. The $1/e^2$ diameters of the focused pump and probe beams are ~10.2 and ~6.2 μm, respectively, at the sample surface.

We utilize the amplitude $\sqrt{{V_{in}}^2 + {V_{out}}^2}$ of the in-phase $V_{in}(t)$ and out-of-phase $V_{out}(t)$ components of the thermoreflectance signal detected by the lock-in amplifier, which is essentially the amplitude of the surface temperature response (i.e., steady periodic temperature oscillations at the sample surface) to the pump heating, to monitor the surface temperature decay over the delay time from 0 to 3.5 ns. The time dependence of the measured amplitude data is compared with that of an analytical solution to the three-dimensional radial-symmetric heat diffusion equation for a multilayer stack of materials to determine unknown thermal parameters [12]. A nonlinear least-squares curve-fitting routine is employed to extract the unknown parameters by minimizing the deviations between the data and the model prediction. We validated the accuracy of our TDTR system with SiO_2 and single crystalline Si reference samples and found values (1.39 ± 0.4 W m^{-1} K^{-1} for SiO_2 and 145 ± 15 W m^{-1} K^{-1} for Si) that are within 2% of literature values for both materials. Further details of the TDTR setup that is used in this study can be found in Refs. [15] and [16]. For more general and detailed descriptions of the TDTR methodology and data analysis, including advantages and limitations of the methodology, see Refs. [12–14].

The multilayer thermal diffusion model contains many parameters, including the thicknesses, thermal conductivities, and volumetric heat capacities of the Al and YSZ layers and the thermal conductivity and volumetric heat capacity of the Si substrate, along with the thermal boundary resistances across the Al/YSZ and YSZ/Si interfaces. For each sample, we determine the Al and YSZ layer thicknesses from cross-sectional TEMs (Fig. 1). The uncertainty in the thickness measurement is estimated to be less than 5%. The thermal conductivity of the Al layer is estimated to be 123 ± 14 W m^{-1} K^{-1} from four-probe measurements of the in-plane electrical resistivity and the use of the Wiedemann-Franz law. The volumetric heat capacity of the Al layer is taken from literature to be 2.43 MJ m^{-3} K^{-1} [17], while that of the YSZ layer is estimated to be 2.55 ± 0.07 MJ m^{-3} K^{-1} from the product of the measured density (5.4–5.7 g cm^{-3}) [3] and the specific heat (0.45976 J g^{-1} K^{-1}) taken form the literature [18]. The thermal conductivity of the (p-doped) Si substrate is measured separately to be 110 ± 12 W m^{-1} K^{-1} using TDTR on the (p-doped) Si substrate coated with a 54-nm-thick Al film. The volumetric heat capacity of the Si substrate is taken from literature to be 1.65 MJ m^{-3} K^{-1} [19,20]. We thus have three unknown parameters in the multilayer thermal diffusion model: (i) the thermal boundary resistance across the Al/YSZ interface (TBR_{Al-YSZ}), (ii) the thermal conductivity of the YSZ layer (k_{YSZ}), and (iii) the thermal boundary resistance across the YSZ/Si interface (TBR_{YSZ-Si}). Here, we extract TBR_{Al-YSZ} and k_{YSZ} by performing a two-parameter fit of the multilayer thermal model to the measured data, while assuming a range of values from 0 to 15 m^2 K GW^{-1} for TBR_{YSZ-Si}. As we discuss in the next section, sensitivity analysis shows that our measurements are most sensitive

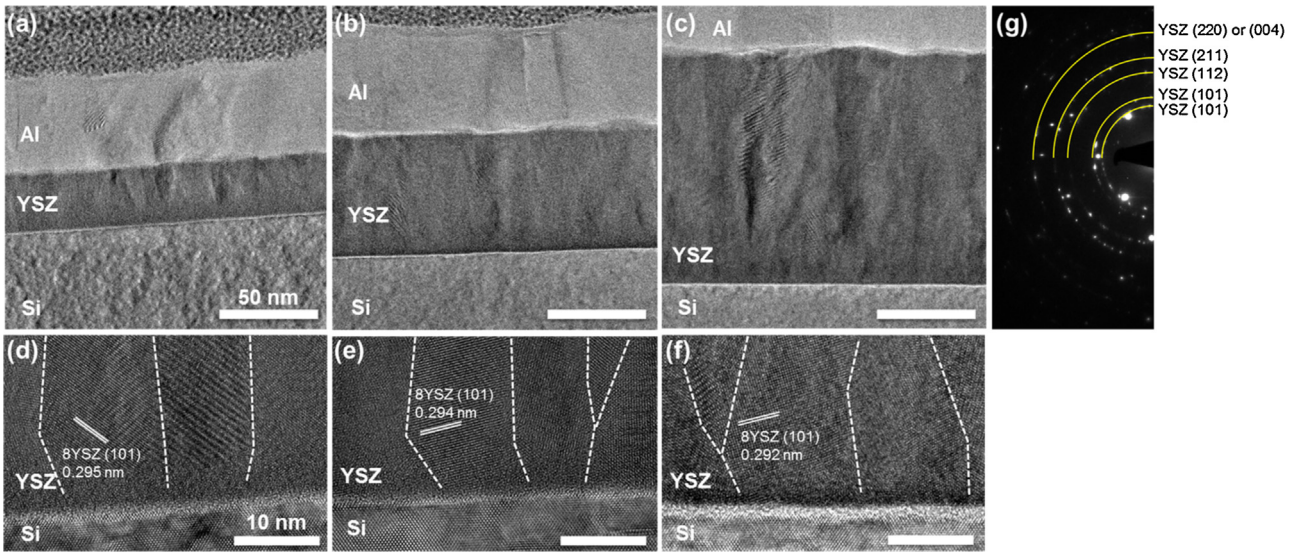

Fig. 2. ((a)–(f)) Cross-sectional TEM images of ALD YSZ films at low magnification ((a) 35 nm, (b) 61 nm, and (c) 138 nm samples) and at high magnification near the YSZ-Si interface ((a) 35 nm, (b) 61 nm, and (c) 138 nm samples), and (g) the SAD pattern of the 138 nm sample.

to the thermal conductivity of the YSZ films while least sensitive to the thermal boundary resistance at the YSZ/Si interface.

3. Results

The TDTR measurement sensitivity to a parameter β in the multilayer thermal model is standardly defined as the logarithmic derivative of the TDTR signal R (either the amplitude $\sqrt{V_{in}{}^2 + V_{out}{}^2}$ or ratio $-V_{in}/V_{out}$) with respect to β: $S_\beta = \partial \ln(R)/\partial \ln(\beta)$ [13–16,21]. Fig. 3(a) plots the sensitivity of the amplitude signal to the three unknown parameters (TBR_{Al-YSZ}, k_{YSZ}, and TBR_{YSZ-Si}) for the three different thickness samples. The values of the sensitivity are evaluated as a function of pump-probe delay time and at the 6 MHz pump modulation frequency. To calculate the sensitivity of the 6 MHz amplitude data, we use best-fit values for TBR_{Al-YSZ} and k_{YSZ} for each sample. As a value of TBR_{YSZ-Si}, we assume 7.5 m^2 K GW^{-1}, which is a median of the assumed range for this resistance.

As illustrated in Fig. 3(a), high measurement sensitivity to k_{YSZ} in our experiments is reflected by large relative magnitude of the sensitivity to k_{YSZ} over most of the delay time for all three samples. The sensitivity to TBR_{Al-YSZ} is much lower than that to k_{YSZ} for all three samples, but TBR_{Al-YSZ} is allowed to vary together with k_{YSZ} to yield the best fit between the model and the data. The thermal boundary resistance at the Al/YSZ interface is highly dependent upon effects of impurities and contamination on the surface and of surface roughness, as well as of varying concentrations of crystalline imperfections in the near-interfacial region [15,22,23]. The sensitivity to TBR_{YSZ-Si} is almost negligible over most of the delay time for the 61 and 138 nm samples, although for the 35 nm sample the sensitivity values of TBR_{YSZ-Si} is comparable to those of TBR_{Al-YSZ}. The propagation of uncertainty from TBR_{YSZ-Si} into uncertainties of the fitted variables (k_{YSZ} and TBR_{Al-YSZ}) is given by the ratio of the sensitivities to these properties, i.e., $S_{TBR_{YSZ-Si}}/S_{k_{YSZ}}$ and $S_{TBR_{YSZ-Si}}/S_{TBR_{Al-YSZ}}$, multiplied by the uncertainty in TBR_{YSZ-Si}. This leads to relatively large uncertainties in k_{YSZ} and TBR_{Al-YSZ} for the thinnest sample given that the sensitivity to TBR_{YSZ-Si} is weak but not negligible for this sample. The uncertainty in TBR_{YSZ-Si}—owing to the assumed range of values from 0 to 15 m^2 K GW^{-1}—propagates to uncertainties in k_{YSZ} of 27, 11, and 3% for the 35, 61, and 138 nm samples, respectively.

Fig. 3(b) shows the 6 MHz amplitude data along with the best analytical fits for all three YSZ samples. We fit the data over a range of delay time from 0.1 to 3.5 ns to extract k_{YSZ} and TBR_{Al-YSZ} after normalizing the data at a delay time of 0.1 ns. Here we select 0.1 ns as the normalization time to minimize the sensitivity of our data fit to non-equilibrium electron-phonon physics (e.g., electron-phonon coupling effects in the Al transducer layer) occurring within the first few tens of picoseconds after the pump heating. We obtain the YSZ thermal conductivity to be 1.35 ± 0.40 W m^{-1} K^{-1} for the 35 nm sample, 1.41 ± 0.19 W m^{-1} K^{-1} for the 61 nm sample, and 1.49 ± 0.13 W m^{-1} K^{-1} for the 138 nm sample. The Al/YSZ thermal boundary resistances are measured to be 3.6 ± 1.5 m^2 K GW^{-1} for the 35 nm sample, 7.0 ± 0.8 m^2 K GW^{-1} for the 61 nm sample, and 8.8 ± 0.6 m^2 K GW^{-1} for the 138 nm sample. The error bars in the reported data are propagated from uncertainties in the Al thickness and thermal conductivity, YSZ thickness and heat capacity, YSZ/Si thermal boundary resistance, and laser spot sizes. Relatively large uncertainties observed in the data for the thinnest sample are due primarily to the uncertainty in the YSZ/Si thermal boundary resistance, as discussed above.

Utilizing higher measurement sensitivity to the buried YSZ/Si interface at a lower pump modulation frequency [24,25], we perform additional measurements using the ratio signal at 2 MHz. With k_{YSZ} and TBR_{Al-YSZ} fixed to those obtained by fitting the 6 MHz amplitude data, we fit the 2 MHz ratio data and estimate the YSZ/Si thermal boundary resistance to be 2–9 m^2 K GW^{-1}, which indeed lies within the range (i.e., between 0 and 15 m^2 K GW^{-1}) assumed for this resistance in our data fitting procedure. This agreement provides confidence in our measured thermal conductivity values.

4. Discussion

The YSZ thermal conductivity values reported here relatively stay constant with increasing film thickness. This may suggest that the thermal conductivity reduction due to phonon boundary scattering is minimal. A recent study on thermal conductivity of ALD-grown amorphous alumina thin films observed that classical size effects are negligible in these films [26], which have thermal conductivities and thicknesses that are comparable to those of our ALD YSZ films. The insignificance of the size effects in our data suggests that the mean free paths of phonons that are important for carrying heat in ALD YSZ films may be below the thickness of the thinnest film, i.e., 35 nm, at room temperature. This is consistent with the prior observation that the mean free paths of the domi-

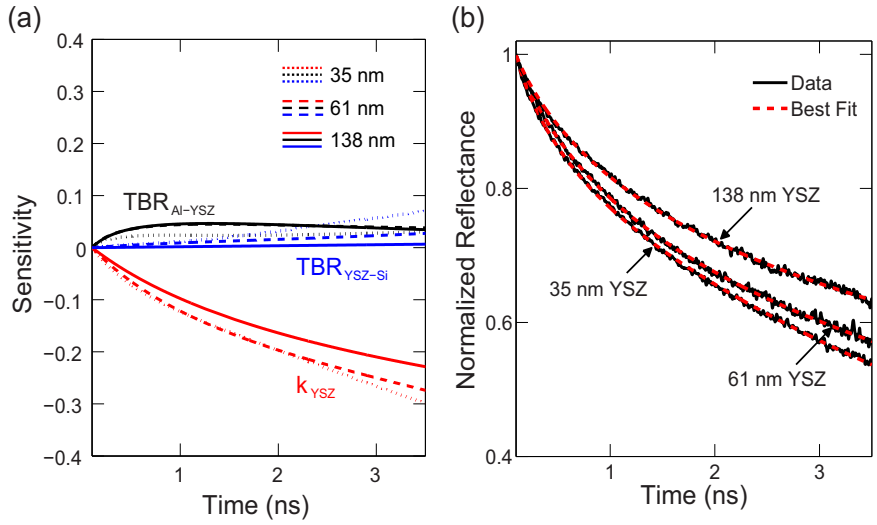

Fig. 3. (a) Sensitivity of the TDTR amplitude signal to the Al/YSZ thermal boundary resistance TBR_{Al-YSZ} (black), the YSZ thermal conductivity k_{YSZ} (red), and the YSZ/Si thermal boundary resistance TBR_{YSZ-Si} (blue) for three different thickness YSZ samples as a function of pump-probe delay time at a pump modulation frequency of 6 MHz. Dotted, dashed, and solid lines represent sensitivity curves for the 35 nm, 61 nm, and 138 nm samples, respectively. Large relative magnitude of the sensitivity to the YSZ thermal conductivity indicates that our measurements are most sensitive to this parameter for all three samples. (b) TDTR amplitude data (black solid lines) along with optimal analytical fits (red dashed lines) for all three YSZ samples at 6 MHz pump modulation frequency. (For interpretation of the references to colour in this figure legend, the reader is referred to the web version of this article.)

nant phonons in nanocrystalline YSZ films are below 30 nm at room temperature [6].

There is a wealth of data in the literature on the thermal conductivity of single crystal YSZ, polycrystalline or nanocrystalline YSZ, and YSZ ceramics [5–9,27–32]. The room-temperature thermal conductivity of fully dense, single crystal YSZ with 4.4–9.7 mol% Y_2O_3 stabilization has been reported to range from 2 to 2.9 $W\,m^{-1}\,K^{-1}$ [5,7,9,27]. High-density, polycrystalline materials with an Y_2O_3 content of 8–10 mol% have a reported thermal conductivity in the range 2–2.3 $W\,m^{-1}\,K^{-1}$ at room temperature [7,28]. A reduced thermal conductivity of 1.7–1.84 $W\,m^{-1}\,K^{-1}$ was measured by Zheng et al. [27] at room temperature using TDTR for 4.5 mol% polycrystalline YSZ specimens prepared by electron beam-physical vapor deposition (EB-PVD). This reduction in thermal conductivity was attributed to the presence of nanometer-scale intra-grain pores and the associated increased phonon scattering. Further reduced thermal conductivity values were reported by Soyez et al. [6] and Yang et al.[29] for nanocrystalline YSZ films, grown by metal-organic chemical vapor deposition (MOCVD), with thicknesses of 0.5–1.2 μm and grain sizes of 10–100 nm. They used the 3ω method to measure these films and reported room-temperature thermal conductivity values approximately from 0.7 to 2 $W\,m^{-1}\,K^{-1}$. The lower end of their reported thermal conductivity values is due primarily to the combined effects of porosity (~10%) and increased phonon-grain boundary scattering at their smallest grain size (10 nm). Many studies [8,30–32] have investigated the thermal conductivity of highly porous YSZ ceramics and reported conductivity values as low as 0.06 $W\,m^{-1}\,K^{-1}$ [8], which corresponds to 77% porosity.

Fig. 4 shows the room-temperature thermal conductivity of YSZ films as a function of film thickness, including our data for ALD YSZ films, the data for polycrystalline, EB-PVD YSZ specimens by Zheng et al. [27], and the data for nanocrystalline, MOCVD YSZ films by Soyez et al. [6], as well as the data for single crystal 8.3 mol% YSZ [5]. Also included is the predicted minimum thermal conductivity for amorphous ~8 mol% YSZ at room temperature calculated using the minimum thermal conductivity model [9]. This model, which describes heat conduction in amorphous materials as a random walk of vibrational energy between localized oscillators, has been successfully used as a baseline model to predict the thermal conductivity of amorphous and highly disordered crystalline materials and therefore sets the lower limit of thermal conductivity [9]. As depicted in Fig. 4, the thermal conductivity values for our ALD YSZ films (1.35–1.5 $W\,m^{-1}\,K^{-1}$) are lower than those of single crystal YSZ with similar composition (2.3 $W\,m^{-1}\,K^{-1}$) [5] and polycrystalline, EB-PVD YSZ specimens (1.7–1.84 $W\,m^{-1}\,K^{-1}$)

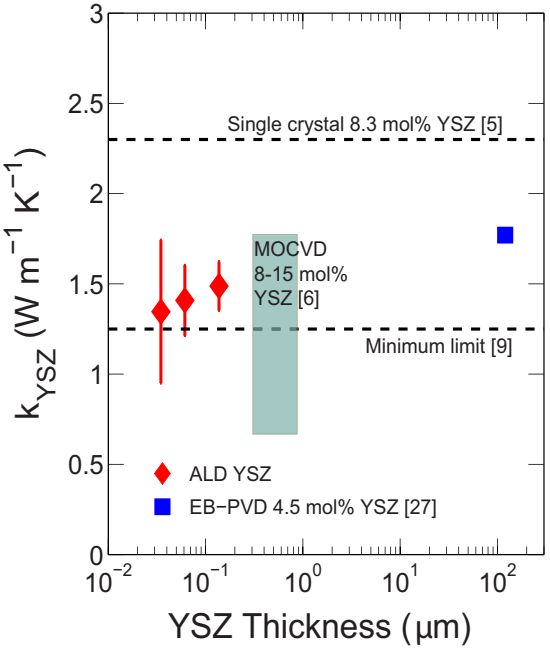

Fig. 4. Thermal conductivity of YSZ films as a function of film thickness at room temperature, including our data for ALD-grown, 8.4 mol% YSZ films (solid diamonds), the data for 4.5 mol% YSZ specimens prepared by electron beam-physical vapor deposition (EB-PVD) (solid square) [27], and the data for nanocrystalline YSZ films deposited by metal-organic chemical vapor deposition (MOCVD) (represented by the shaded area) [6]. The Y_2O_3 content and grain size for the MOCVD-grown, nanocrystalline YSZ films are 8–15 mol% and 10–100 nm, respectively [6]. The data for single crystal 8.3 mol% YSZ [5] and the prediction of the minimum thermal conductivity model for amorphous ~8 mol% YSZ [9] are depicted by the upper and lower dashed lines, respectively.

[27]. The lower end (~0.7 $W m^{-1} K^{-1}$) of YSZ thermal conductivity values reported by Soyez et al. [6] is almost half our reported conductivity values, but their relatively lower values are partly owing to the effect of porosity (~10%). Our ALD YSZ films do not have any physical pores and are thus fully dense. The effects of porosity are therefore not responsible for low thermal conductivity values observed in our ALD YSZ films. It is of note that without any effects of porosity the thermal conductivities of our ALD YSZ films still approach the minimum limit to the thermal conductivity of YSZ (1.25 $W m^{-1} K^{-1}$ (Ref. [9])).

Several studies have investigated the mechanisms of thermal transport in YSZ [5,7,9,29,33]. These studies have revealed that relatively low thermal conductivity values of single crystal and polycrystalline YSZ—which are comparable to that of a glass—are largely due to increased scattering of phonons by vacancies of the oxygen sites in the lattice, as well as by a small spacing between oxygen vacancies [5,7,29,33]. Both are associated with the substitution of two Zr^{4+} ions with two Y^{3+} ions and the introduction of one oxygen vacancy into the zirconia structure to maintain charge neutrality [2,5]. In ~10 mol% YSZ, for example, the percentage of vacancies in the oxygen sites in the lattice is ~4.5%, and the average distance between oxygen vacancies is approximately less than 2 nm [29], which is smaller than the important mean free paths of phonons in YSZ. Enhanced scattering of phonons by grain boundaries for grain sizes that are smaller than or comparable to the important phonon mean free paths in YSZ can further reduce the thermal conductivity [6,29,33]. The presence of pores greatly reduces the thermal conductivity mainly owing to the combined effects of the low thermal conductivity of air—which is trapped in the pores—and the increased phonon scattering by pore boundaries, as evidenced by many experimental observations on highly porous YSZ ceramics [8,30–32]. Cahill et al. [9] used the minimum thermal conductivity model to examine the (minimum) amorphous limit to the thermal conductivity of fully dense YSZ, which was predicted to be 1.25 $W m^{-1} K^{-1}$, as described above. The low thermal conductivity values reported in the present study, which approach the minimum thermal conductivity limit, may be attributed to the increased scattering of phonons by grain boundaries (with the average grain size of ~10 nm) [34,35], as well as by atomic disorder in the amorphous phase within the films.

Of further interest is the thermal conductivity of YSZ at temperatures higher than room temperature, which are relevant to thermal insulation applications. It has been shown that the thermal conductivity of single crystal YSZ and polycrystalline or nanocrystalline YSZ is glasslike for Y_2O_3 concentrations comparable to or higher than 8 mol% [6,7,9,29]. The thermal conductivity of single crystal YSZ and polycrystalline YSZ slowly increases with increasing temperature for temperatures higher than room temperature [7,9], which is characteristic of amorphous and highly defective crystalline materials [9]. The thermal conductivity of nanocrystalline YSZ has been reported to slightly increase [29] or relatively stay constant [6] with increasing temperature. Yang et al. [29] reported that the thermal conductivity of their nanocrystalline sample with a grain size of 10 nm—the smallest grain-sized one among their samples—increases by ~10% over the temperature range 300–500 K, which is very similar to the prediction of the minimum thermal conductivity model. Based on these past findings, we expect the thermal conductivity of our ALD YSZ films to slightly increase with temperature above room temperature.

The ALD growth method can provide nanometer-scale, uniform and isotropic film deposition over three-dimensional substrates without pinholes. This nature of ALD film growth is extremely valuable when it comes to uniform and conformal coating of the surface of complex, three-dimensional nanostructures, which is an essential feature required for a wide variety of modern nanoscale electronic and energy conversion devices. The combination of the growth nature of ALD and low thermal conductivity values observed here may suggest the potential benefits of using ALD YSZ for various thermal insulation applications in these devices.

5. Conclusions

We have performed experimental investigation of the thermal conductivity of ALD-grown, 8.4 mol% YSZ films of thickness down to 35 nm using TDTR. The measured thermal conductivities, which are nearly independent of film thickness, are approximately 1.35–1.5 $W m^{-1} K^{-1}$ at room temperature and approach the minimum limit to the thermal conductivity of YSZ. Given the fully dense nature of our ALD YSZ films, we note that without any effects associated with porosity the thermal conductivities measured here still approach the minimum thermal conductivity limit. Our measured thermal conductivities are, to the best of our knowledge, the lowest thermal conductivity ever reported for nonporous YSZ. This may be associated with increased phonon scattering by grain boundaries with an average grain sizes of ~10 nm, as well as by the random and disordered nature of the amorphous phase within the films. The low thermal conductivities observed here, combined with the fact that ALD can offer conformal and uniform coating of the surface of complex, three-dimensional nanostructures, may suggest the potential benefits of using ALD YSZ as a thermal insulation material in a variety of modern nanoscale electronic and energy conversion devices.

Acknowledgements

This work was supported by the National Research Foundation of Korea (NRF) grants funded by the Korea government (MSIP) (No. 2016R1C1B2015317 and No. NRF-2015R1D1A1A01058963).

References

[1] N.P. Padture, M. Gell, E.H. Jordan, Thermal barrier coatings for gas-turbine engine applications, Science 296 (2002) 280–284.
[2] D.R. Clarke, S.R. Phillpot, Thermal barrier coating materials, Mater. Today 8 (2005) 22–29.
[3] J.H. Shim, C.C. Chao, H. Huang, F.B. Prinz, Atomic layer deposition of yttria-stabilized zirconia for solid oxide fuel cells, Chem. Mater. 19 (2007) 3850–3854.
[4] J. An, Y.B. Kim, J. Park, T.M. Gur, F.B. Prinz, Three-dimensional nanostructured bilayer solid oxide fuel cell with 1.3 W/cm^2 at 450 °C, Nano Lett. 13 (2013) 4551–4555.
[5] J.F. Bisson, D. Fournier, M. Poulain, O. Lavigne, R. Mévrel, Thermal conductivity of yttria-zirconia single crystals, determined with spatially resolved infrared thermography, J. Am. Ceram. Soc. 83 (2000) 1993–1998.
[6] G. Soyez, J.A. Eastman, L.J. Thompson, G.R. Bai, P.M. Baldo, A.W. McCormick, R.J. DiMelfi, A.A. Elmustafa, M.F. Tambwe, D.S. Stone, Grain-size-dependent thermal conductivity of nanocrystalline yttria-stabilized zirconia films grown by metal-organic chemical vapor deposition, Appl. Phys. Lett. 77 (2000) 1155–1157.
[7] K.W. Schlichting, N.P. Padture, P.G. Klemens, Thermal conductivity of dense and porous yttria-stabilized zirconia, J. Mater. Sci. 36 (2001) 3003–3010.
[8] G. Pia, L. Casnedi, U. Sanna, Porosity and pore size distribution influence on thermal conductivity of yttria-stabilized zirconia: experimental findings and model predictions, Ceram. Int. 42 (2016) 5802–5809.
[9] D.G. Cahill, S.K. Watson, R.O. Pohl, Lower limit to the thermal conductivity of disordered crystals, Phys. Rev. B 46 (1992) 6131–6140.
[10] C. Bernay, A. Ringuedé, P. Colomban, D. Lincot, M. Cassir, Yttria-doped Zirconia thin films deposited by atomic layer deposition ALD: a structural, morphological and electrical characterisation, J. Phys. Chem. Solids 64 (2003) 1761–1770.
[11] X. Bokhimi, A. Morales, A. Garcıa-Ruiz, T.D. Xiao, H. Chen, P.R. Strutt, Transformation of yttrium-doped hydrated zirconium into tetragonal and cubic nanocrystalline zirconia, J. Solid State Chem. 142 (1999) 409–418.
[12] D.G. Cahill, Analysis of heat flow in layered structures for time-domain thermoreflectance, Rev. Sci. Instrum. 75 (2004) 5119–5122.
[13] A.J. Schmidt, X. Chen, G. Chen, Pulse accumulation, radial heat conduction, and anisotropic thermal conductivity in pump-probe transient thermoreflectance, Rev. Sci. Instrum. 79 (2008) 114902.

[14] D.G. Cahill, P.V. Braun, G. Chen, D.R. Clarke, S. Fan, K.E. Goodson, P. Keblinski, W.P. King, G.D. Mahan, A. Majumdar, H.J. Maris, S.R. Phillpot, E. Pop, L. Shi, Nanoscale thermal transport. II. 2003–2012, Appl. Phys. Rev. 1 (2014) 011305.
[15] J. Cho, Y. Li, W.E. Hoke, D.H. Altman, M. Asheghi, K.E. Goodson, Phonon scattering in strained transition layers for GaN heteroepitaxy, Phys. Rev. B 89 (2014) 115301.
[16] J. Cho, D. Francis, D.H. Altman, M. Asheghi, K.E. Goodson, Phonon conduction in GaN-diamond composite substrates, J. Appl. Phys. 121 (2017) 055105.
[17] W.F. Giauque, P.F. Meads, The heat capacities and entropies of aluminum and copper from 15 to 300 K, J. Am. Chem. Soc. 63 (1941) 1897–1901.
[18] T. Tojo, T. Atake, T. Mori, H. Yamamura, Heat capacity and thermodynamic functions of zirconia and yttria-stabilized zirconia, J. Chem. Thermodyn. 31 (1999) 831–845.
[19] M. Asheghi, K. Kurabayashi, R. Kasnavi, K.E. Goodson, Thermal conduction in doped single-crystal silicon films, J. Appl. Phys. 91 (2002) 5079–5088.
[20] P. Flubacher, A.J. Leadbetter, J.A. Morrison, Heat capacity of pure silicon and germanium and properties of their vibrational frequency spectra, Philos. Mag. 4 (1959) 273–294.
[21] B.C. Gundrum, D.G. Cahill, R.S. Averback, Thermal conductance of metal-metal interfaces, Phys. Rev. B 72 (2005) 245426.
[22] P.E. Hopkins, L.M. Phinney, J.R. Serrano, T.E. Beechem, Effects of surface roughness and oxide layer on the thermal boundary conductance at aluminum/silicon interfaces, Phys. Rev. B 82 (2010) 085307.
[23] C.S. Gorham, K. Hattar, R. Cheaito, J.C. Duda, J.T. Gaskins, T.E. Beechem, J.F. Ihlefeld, L.B. Biedermann, E.S. Piekos, D.L. Medlin, P.E. Hopkins, Ion irradiation of the native oxide/silicon surface increases the thermal boundary conductance across aluminum/silicon interfaces, Phys. Rev. B 90 (2014) 024301.
[24] S.T. Huxtable, D.G. Cahill, L.M. Phinney, Thermal contact conductance of adhered microcantilevers, J. Appl. Phys. 95 (2004) 2102–2108.
[25] P.E. Hopkins, J.C. Duda, S.P. Clark, C.P. Hains, T.J. Rotter, L.M. Phinney, Balakrishnan, G: Effect of dislocation density on thermal boundary conductance across GaSb/GaAs interfaces, Appl. Phys. Lett. 98 (2011) 161913.
[26] C.S. Gorham, J.T. Gaskins, G.N. Parsons, M.D. Losego, P.E. Hopkins, Density dependence of the room temperature thermal conductivity of atomic layer deposition-grown amorphous alumina (Al_2O_3), Appl. Phys. Lett. 104 (2014) 253107.
[27] X. Zheng, D.G. Cahill, J.C. Zhao, Thermal conductivity imaging of thermal barrier coatings, Adv. Eng. Mater. 7 (2005) 622–626.
[28] D.P.H. Hasselman, L.F. Johnson, L.D. Bentsen, S. RAHMATHULLAH, L.L. HONG, M.V. Swain, Thermal diffusivity and conductivity of dense polycrystalline ZrO_2 ceramics: a survey, Am. Ceram. Soc. Bull. 66 (1987) 799–806.
[29] H.S. Yang, G.R. Bai, L.J. Thompson, J.A. Eastman, Interfacial thermal resistance in nanocrystalline yttria-stabilized zirconia, Acta. Mater. 50 (2002) 2309–2317.
[30] B. Nait-Ali, K. Haberko, H. Vesteghem, J. Absi, D.S. Smith, Thermal conductivity of highly porous zirconia, J. Eur. Ceram. Soc. 26 (2006) 3567–3574.
[31] H. Zhao, F. Yu, T.D. Bennett, H.N. Wadley, Morphology and thermal conductivity of yttria-stabilized zirconia coatings, Acta. Mater. 54 (2006) 5195–5207.
[32] L. Hu, C.A. Wang, Y. Huang, Porous yttria-stabilized zirconia ceramics with ultra-low thermal conductivity, J. Mater. Sci. 45 (2010) 3242–3246.
[33] P.K. Schelling, S.R. Phillpot, Mechanism of thermal transport in zirconia and yttria-stabilized zirconia by molecular-dynamics simulation, J. Am. Ceram. Soc. 84 (2001) 2997–3007.
[34] J. Lee, Z. Li, J.P. Reifenberg, S. Lee, R. Sinclair, M. Asheghi, K.E. Goodson, Thermal conductivity anisotropy and grain structure in $Ge_2Sb_2Te_5$ films, J. Appl. Phys. 109 (2011) 084902.
[35] Z. Li, J. Lee, J.P. Reifenberg, M. Asheghi, R.G. Jeyasingh, H.P. Wong, K.E. Goodson, Grain boundaries, phase impurities, and anisotropic thermal conduction in phase-change memory, IEEE Electron Device Lett. 32 (2011) 961–963.